

Spectroscopy of light atoms and bounds on physics beyond the standard model

R. M. Potvliege

Department of Physics, Durham University, South Road, Durham DH1 3LE, UK

E-mail: r.m.potvliege@durham.ac.uk

Abstract. Newly calculated bounds on the strength of the coupling of an electron to a proton or a neutron by a fifth force are presented. These results are derived from the high precision spectroscopic data currently available for hydrogen, deuterium, helium-3 and helium-4. They do not depend on specific assumptions on how the interaction would couple to a deuteron compared to a proton or would couple to an α particle compared to a helion. They depend on its coupling to a muon, but not in a significant way for carrier masses below 100 keV if one assumes that the strength of the interaction with a muon would be of a similar order of magnitude as the strength of the interaction with an electron in that mass region.

1. Introduction

A growing number of atomic systems are relevant in the ongoing search for a new physics interaction in view of the very high level of precision achieved in their spectroscopy. Two main approaches have been considered on this front in regard to the possible existence of a fifth force. One is to search for departures from the predictions of the standard model for differences in transition frequencies between different isotopes of a same species. This approach is based on the analysis of what is called King plots nonlinearities [1]. It has been recently applied to ytterbium atoms, ytterbium ions and calcium ions ([2, 3, 4] and references therein). The other is to search for departures from the predictions of the standard model in one- or two-electron systems whose transition frequencies can be both measured and calculated to a suitably high precision [5, 6, 7]. This second approach has been explored in some detail in [8], in particular in regard to the prospects offered by transitions in hydrogen, deuterium, helium-3 and helium-4 for setting bounds on the strength of a fifth force, and also in our more recent work on bounds based on hydrogen and deuterium spectroscopy [9, 10]. It has been extended to a broader variety of atomic systems and experimental data for specific new physics models in [11].

We revisit and continue some of these earlier investigations in the present article, in the light of recent experimental and theoretical advances in the spectroscopy of light elements and their muonic counterparts [12, 13, 14, 15, 16, 17, 18, 19, 20]. Specifically, we consider the possibility that a new physics interaction impart a potential energy $V_{\text{NP}}(r)$ to an electron or muon located at a distance r from a hydrogen or helium nucleus, with

$$V_{\text{NP}}(r) = (-1)^{s+1} \frac{g_l g_N}{4\pi} \frac{1}{r} \exp(-m_{X_0} r) \quad (1)$$

in natural units. Here m_{X_0} is the mass of the new physics boson mediating the interaction, s is the spin of this boson, and g_l and g_N are two dimensionless constants ($g_l \equiv g_e$ for an electron, $g_l \equiv g_\mu$ for a muon, $g_N \equiv g_p$ for hydrogen-1, $g_N \equiv g_d$ for deuterium, $g_N \equiv g_h$ for helium-3 and $g_N \equiv g_\alpha$ for helium-4). A large class of new physics models give rise to such a contribution to the Hamiltonian. As is commonly done in this context, we will assume that

$$g_n = g_d - g_p = g_\alpha - g_h, \quad (2)$$

where g_n is the coupling constant for a neutron. Our main results are new upper bounds on the products $g_e g_p$ and $g_e g_n$. While we make use of the nuclear rms charge radii derived from Lamb shift measurements on the muonic species, we take into account the possibility that a new physics interaction might need to be taken into account in the calculation of these charge radii. We do not use scattering data in view of the difficulties with deriving charge radii from these results [21, 22].

We calculate bounds based on hydrogen and deuterium spectroscopy in Section 2, deriving them either by a global fit of the data to theoretical models [9, 10] or in a simpler analysis of the isotope shift of the 1s – 2s interval [8]. The latter approach is extended to helium in Section 3.

2. Bounds derived from hydrogen and deuterium spectroscopy

2.1. Consistency of the data

The proton rms charge radius (r_p), the deuteron rms charge radius (r_d) and the Rydberg constant (\mathcal{R}) are co-determined from a set of experimental and theoretical results including, in particular, high precision spectroscopic measurements in muonic hydrogen and deuterium (μH , μD) and in electronic hydrogen and deuterium (eH, eD) [23]. In principle, these data may be significantly affected by the hypothetical fifth force considered in the present work. As a consequence, setting bounds on the strength of this force involves redetermining these quantities. However, doing so is hampered by well known discrepancies and inconsistencies: discrepancies between the measurements on the muonic species and the measurements on the electronic species and inconsistencies between the latter. These differences result, *inter alia*, in a significant scatter in the values of r_p derived from these measurements — see, e.g., Fig. 1(a) and similar figures in [24, 25]. The measurements in μH yield a value of r_p of 0.84060(39) fm [15, 26] (we denote this value by $r_{p,\mu\text{H}}$ in the following). The values derived from measurements in eH have a larger uncertainty. The most precise published so far are based on the $1s - 3s$, $2p - 2s$, $2s - 4p$ or $2s_{1/2} - 8d_{5/2}$ intervals, in conjunction with previous measurements of the $1s - 2s$ interval [27, 28]. A value of 0.8482(38) fm can be derived from the most recent measurement of the $1s - 3s$ interval [29]. It is in 2σ tension both with $r_{p,\mu\text{H}}$ and also with the still larger value of 0.877(13) fm derived from an independent measurement of the same interval [30]. A recent measurement of the $2s_{1/2} - 8d_{5/2}$ interval yield a value of 0.8584(51) fm, larger than and in 3.5σ tension with $r_{p,\mu\text{H}}$ [24] and differing by 2.2σ from the still larger value implied by the results of a previous measurement of that interval [31]. On the other hand, the values of r_p based on the recent measurements of the $2p - 2s$ and $2s - 4p$ intervals, respectively 0.833(10) fm [32] and 0.8335(95) fm [33], are in good agreement with each other and with $r_{p,\mu\text{H}}$. The value of r_d derived from measurements in muonic deuterium is also in significant tension with the values that can be derived from the spectroscopy of electronic deuterium [34].

By contrast, there is now excellent agreement between measurements on the muonic species and measurements on the electronic species in regard to the difference $r_d^2 - r_p^2$, when this difference is derived directly from the isotope shift of the $1s - 2s$ interval of eH and eD [15] — see, e.g., Fig. 1(b). (The experimental uncertainty on this difference is particularly small for the electronic species, owing both to the particularly high precision with which this isotope shift was measured [35] and to the cancellation of theoretical errors in the final results [12, 36].

2.2. General approach: Method

Energy differences between states of electronic hydrogen or deuterium are usually expressed as transition frequencies, e.g., ν_{ba} for the energy difference between a state b and a state a . Theoretically, these transition frequencies have the following general

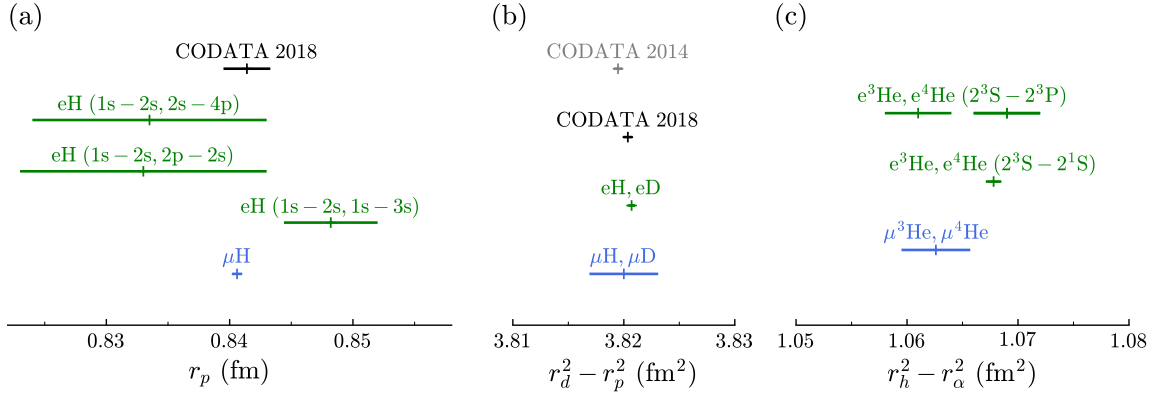


Figure 1. (a) The proton rms charge radius, r_p . (b) The difference $r_d^2 - r_p^2$. (c) The difference $r_h^2 - r_\alpha^2$. From top to bottom in (a): Value recommended by CODATA (2018 adjustment) [23]; value derived from measurements of the 1s – 2s and 2s – 4p intervals in eH [33]; value derived from measurements of the 1s – 2s interval and of the 2p – 2s Lamb shift in eH [32]; value derived from measurements of the 1s – 2s and 1s – 3s intervals in eH [29]; value derived from measurements in muonic hydrogen [15]. From top to bottom in (b): Value recommended by CODATA (2014 adjustment) [38]; values recommended by CODATA (2018 adjustment) [23]; result derived from the isotope shift of the 1s – 2s interval in the electronic species [12]; value derived from measurements in muonic hydrogen and muonic deuterium [15]. From top to bottom in (c): Values derived from the isotope shift of the $2^3S - 2^3P$ interval in the electronic species as measured by Shiner *et al* [40, 42] (left) or as measured by Cancio Pastor *et al* [40, 43, 44] (right); value derived from the isotope shift of the $2^3S - 2^1S$ interval in the electronic species [16, 17]; value derived from measurements in muonic ^3He and muonic ^4He [13, 18] as redetermined in [19].

form within the standard model,

$$\nu_{ba}^{\text{SM}}(\mathcal{R}, r_p, r_d) = \mathcal{R} \tilde{\nu}_{ba}^g + r_p^2 \tilde{\nu}_{ba}^{\text{ps}} + r_d^2 \tilde{\nu}_{ba}^{\text{ds}} + \nu_{ba}^{\text{oc}}, \quad (3)$$

where ν_{ba}^{oc} , $\tilde{\nu}_{ba}^g$, $\tilde{\nu}_{ba}^{\text{ps}}$, $\tilde{\nu}_{ba}^{\text{ds}}$ and ν_{ba}^{oc} are constants which do not need to be calculated with highly precise values of \mathcal{R} , r_p and r_d . The term $\mathcal{R} \tilde{\nu}_{ba}^g$ accounts for the gross structure of the spectrum as predicted by the non-relativistic theory to leading order in the fine structure constant, the terms $r_p^2 \tilde{\nu}_{ba}^{\text{ps}}$ and $r_d^2 \tilde{\nu}_{ba}^{\text{ds}}$ account for the bulk of the dependence of ν_{ba} on the nuclear charge radii, and the term ν_{ba}^{oc} accounts for all the other relevant relativistic and QED corrections. The deuteron size term $r_d^2 \tilde{\nu}_{ba}^{\text{ds}}$ is absent for transitions in hydrogen-1, and conversely the proton size term $r_p^2 \tilde{\nu}_{ba}^{\text{ps}}$ is absent for transitions in deuterium. Similar expressions relate r_p and r_d to the Lamb shift in muonic hydrogen and muonic deuterium.

Given these expressions, the values of \mathcal{R} , r_p and r_d must be such that these theoretical energy differences match the measured intervals within experimental and theoretical errors. Namely, they must be such that

$$\nu_{b_i a_i}^{\text{SM}}(\mathcal{R}, r_p, r_d) \doteq \nu_{b_i a_i}^{\text{exp}}, \quad i = 1, 2, 3, \dots \quad (4)$$

over all the transitions considered if the possibility of a new physics interaction is ignored. (Since this set of equations is overdetermined in most cases of interest, the resulting values of \mathcal{R} , r_p and r_d normally need to be obtained by χ^2 -fitting, as the symbol \doteq indicates [37].) A hypothetical fifth force would contribute a new physics shift of $\nu_{b_i a_i}^{\text{NP}}$ to the measured interval, for a transition between a state a_i and a state b_i . If one assumes the existence of this interaction, comparing experiment to the standard model then involves finding values of \mathcal{R} , r_p and r_d such that

$$\nu_{b_i a_i}^{\text{SM}}(\mathcal{R}, r_p, r_d) \doteq \nu_{b_i a_i}^{\text{exp}} - \nu_{b_i a_i}^{\text{NP}}, \quad i = 1, 2, 3, \dots \quad (5)$$

Requiring the existence of values of \mathcal{R} , r_p and r_d consistent with these equations and with the measurements in muonic hydrogen and muonic deuterium is the main constraint we use for setting bounds on the strength of this fifth force. We calculate the necessary values of ν_{ba}^{oc} , $\tilde{\nu}_{ba}^{\text{g}}$, $\tilde{\nu}_{ba}^{\text{ps}}$, $\tilde{\nu}_{ba}^{\text{ds}}$ and ν_{ba}^{oc} as explained in Appendix C of [9] and Appendix B of [10]. Like [10], we also follow [14] and [26] for the muonic species. We calculate the new physics shifts ν_{ba}^{NP} as outlined in Appendix A of the present article.

We set a further constraint on the strength of this hypothetical new physics interaction by requiring that the above calculations of r_p and r_d result in a value of $r_d^2 - r_p^2$ consistent with the value determined from the experimental isotope shift of the 1s – 2s interval in the electronic species. Specifically, we require that the experimental isotope shift of that interval matches its theoretical prediction, taking into account the possibility of a new physics contribution. As is explained in Appendix C of [10], this requirement can be expressed by the inequality

$$|\Delta| \leq 1.96 \sigma_\Delta, \quad (6)$$

where

$$\Delta = 5233.27(42) \text{ kHz} + \Delta\nu_{2s1s}^{\text{NP}} - \frac{7\alpha^4 m_e c^2}{12h\lambda_C^2} \left[\left(\frac{m_r^{\text{eD}}}{m_e} \right)^3 r_d^2 - \left(\frac{m_r^{\text{eH}}}{m_e} \right)^3 r_p^2 \right], \quad (7)$$

and σ_Δ is the combined experimental and theoretical error on the value of Δ . In this last equation, h is Planck's constant, α is the fine structure constant, λ_C is the reduced Compton wavelength, m_e is the electron mass, m_r^{eH} and m_r^{eD} are the reduced masses of the respective isotopes, and $\Delta\nu_{2s1s}^{\text{NP}}$ is the hypothetical contribution of the new physics interaction to the experimental isotope shift of the 1s – 2s interval.

To obtain bounds on the products $g_e g_p$ and $g_e g_n$, we χ^2 -fit the model to the data for set values of the mass m_{X_0} , of the ratio g_d/g_p and of the ratio g_μ/g_e , subject to the aforementioned constraints and to the assumption that $g_d = g_p + g_n$. Doing so results in upper bounds on $|g_e g_p|$ and $|g_e g_n|$, namely bounds $|g_e g_p|_{\text{max}}$ and $|g_e g_n|_{\text{max}}$ depending both on the carrier mass and on the ratios g_d/g_p and g_μ/g_e .[‡] We take $|g_e g_p|_{\text{max}}$ and $|g_e g_n|_{\text{max}}$ to be the largest values of $|g_e g_p|$ and $|g_e g_n|$ for which $Q(\chi^2, \nu) \geq 0.05$ where $Q(\chi^2|\nu)$ is the upper tail cumulative distribution function for the relevant number of

[‡] These two quantities are not independent since $g_n = (g_d/g_p - 1)g_p$ in view of Eq. (2).

degrees of freedom, ν (the boundary value of 0.05 corresponds to a confidence level of 95% that the data exclude the possibility that $|g_e g_p|$ and $|g_e g_n|$ are larger than the values of, respectively, $|g_e g_p|_{\max}$ and $|g_e g_n|_{\max}$ obtained by the fitting procedure). For each value of m_{X_0} and of g_μ/g_e , we then take the absolute upper bound on $|g_e g_p|$ to be the highest value of $|g_e g_p|_{\max}$ over the range $-\infty < g_d/g_p < \infty$, and similarly for the absolute upper bound on $|g_e g_n|$. We found that varying g_d/g_p between -1 and 3 was sufficient for finding these absolute maxima for most values of m_{X_0} .

2.3. General approach: Results for $g_\mu = g_e$

Proceeding as described in Section 2.2 yields bounds depending both on the value of the ratio g_μ/g_e and on the experimental data used in the calculation. We first consider results obtained under the lepton universality assumption that $g_\mu = g_e$. The bounds represented by the solid black curves in Figs. 2 and 3 are based on the World spectroscopic data as in [10].§ Previous results are also shown, for comparison. The shaded region in Fig. 2 identifies the values of $g_e g_p$ excluded by the spectroscopy of eH alone [10]. The shaded region in Fig. 3 identifies the values of $g_e g_n$ excluded by an analysis of neutron scattering data and measurements of the anomalous magnetic moment of the electron [1, 8]. The solid green curves, in Fig. 3, show the bounds on $g_e g_n$ derived in [2] from a generalized King plots analysis of the spectroscopy of Yb and Yb⁺ (similar but slightly more constraining bounds have been obtained in still more recent analyses of King plots nonlinearities of isotope shifts of ytterbium and calcium transitions [3, 4]).

Tighter bounds can be obtained by using a smaller set of experimental data in the fitting procedure. Only using the μ H and μ D data, the highly precise value of 1s – 2s transition frequency in eH [27] and the isotope shift of this interval [35] gives the tightest bounds on $g_e g_n$ that can be derived from hydrogen and deuterium spectroscopy [8, 10]. These bounds are represented by long-dashed curves in Fig. 3.|| As seen from the graphs, they are significantly lower than the bounds based on the whole World data set and those based on King plots nonlinearities, except in the high mass region.

The corresponding 1s – 2s bounds on $g_e g_p$ are considerably weaker than those based on the World data (Fig. 2), though, because a calculation based merely on that interval does not strongly constrain $g_e g_p$ when $g_d \approx g_p$ [10]. When $g_d = g_p$, indeed, the isotope shift depends on the strength of the new physics interaction only because of the difference in reduced mass between the two isotopes. This lack of sensitivity can be remedied by adding the transition frequency of a different interval to the data set, as long as the

§ As in [10, 23], we alleviated difficulties in the χ^2 -fitting caused by the internal inconsistencies of this data set by magnifying all the experimental errors by 60% when calculating these bounds and those represented by the dotted curves. The errors were not magnified for the other bounds discussed in this article.

|| These results are practically identical to those represented by the “1S–2S HD (muonLS)” curves in Figs. 1 and 3 of [8], which in effect were showing the $\pm 1.96 \sigma_{g_e g_n}$ confidence interval defined in Section 2.5 below rather than bounds as discussed here.

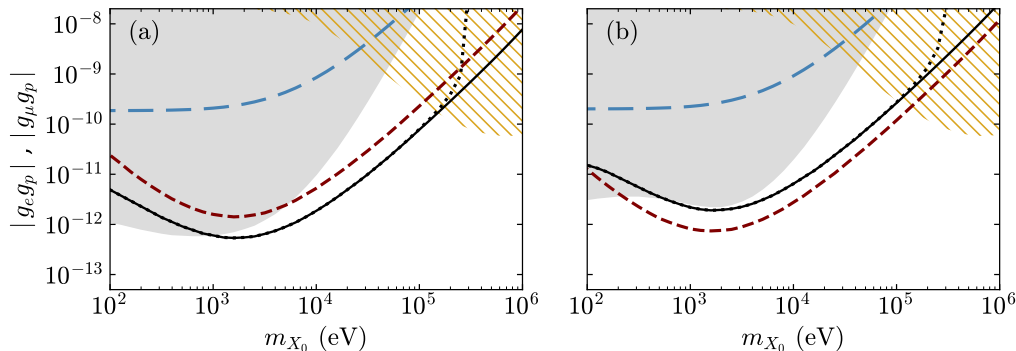


Figure 2. Bounds on $g_e g_p$, (a) for $(-1)^{s+1} g_e g_p < 0$, (b) for $(-1)^{s+1} g_e g_p > 0$. Shaded areas: regions excluded by the spectroscopy of eH [10]. Solid curves: bounds based on the World spectroscopic data, assuming that $g_\mu = g_e$. Dotted curves: the same bounds as the solid curves but for the less constraining assumption that $-1 \leq g_\mu \leq 100 g_e$. Long-dashed curves: bounds based only on the 1s – 2s interval of eH, the isotope shift of the 1s – 2s interval and the μH and μD Lamb shifts, assuming that $g_\mu = g_e$. Short-dashed curves: the same as the long-dashed curves when the 2s – 4p interval of eH is added to the data set. Hatched areas: values of $|g_\mu g_p|$ for which the new physics interaction between the muon and the proton would shift the $2s_{1/2} - 2p_{3/2}$ interval in muonic hydrogen by more than 5% of the experimental error on the Lamb shift [10].

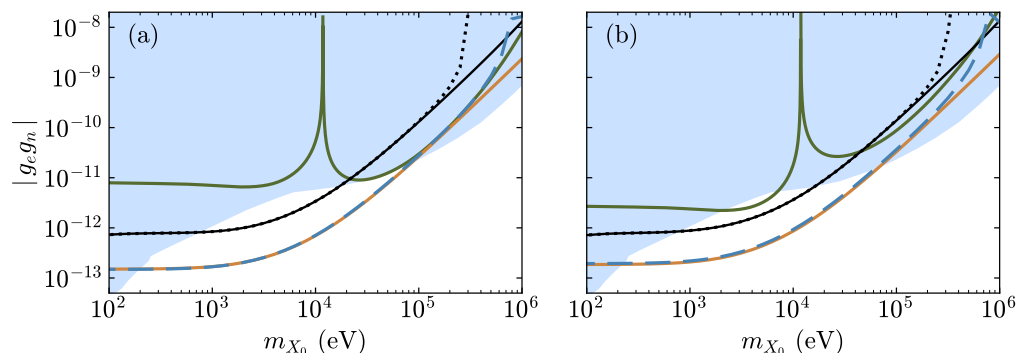


Figure 3. Bounds on $g_e g_n$, (a) for $(-1)^{s+1} g_e g_n < 0$, (b) for $(-1)^{s+1} g_e g_n > 0$. Shaded area: region excluded by neutron scattering data combined with measurements of the anomalous magnetic moment of the electron [1, 8]. Solid green curves: upper bounds derived from the Yb/Yb⁺ isotope shift [2]. Solid black curves, dotted curves and long-dashed curves: as in Fig. 2, here for $g_e g_n$. Solid orange curves, almost identical to the long-dashed curves below 100 keV: upper bounds calculated from Eq. (17).

new physics shift of this interval differs enough from that of the 1s – 2s interval and the experimental error is sufficiently small. For example, and as seen from Fig. 2, adding the 2s – 4p transition frequency measured in eH [33] yields bound comparable or tighter than those based on the World data.

2.4. Dependence on g_μ

How much the results of the previous section depend on the value of g_μ compared to the value of g_e may be inferred from Appendix A of [10], which concerns the impact of a new physics interaction on the determination of r_p and r_d from muonic hydrogen and muonic deuterium spectroscopy. The calculations described in that previous work aimed at delineating the values of $|g_\mu g_p|$ and $|g_\mu g_d|$ above which the interaction might affect the $2s_{1/2} - 2p_{3/2}$ interval significantly (r_p and r_d are derived from the experimental values of that interval). As in [10], we conservatively take “significant” as meaning a shift of more than 5% of the experimental error on the respective Lamb shift. The regions of the $(|g_\mu g_p|, m_{X_0})$ plane in which the impact of a new physics interaction is significant by that definition is represented by hashed areas in Fig. 2. It extends down to $|g_\mu g_p| \approx 2 \times 10^{-8}$ in the low mass region, and, as can be seen in the figure, to slightly below 1×10^{-10} for $m_{X_0} \approx 1$ MeV. Up to 10 keV, $|g_\mu|$ should thus be at least four orders of magnitude larger than $|g_e|$ for invalidating the bounds discussed in the previous section. However, a smaller ratio of $|g_\mu|$ to $|g_e|$ would be sufficient to do so above 10 keV, particularly above 100 keV.

We examined the impact of a possible difference between g_μ and g_e by recalculating the World data bounds under the more general assumption that $-g_e \leq g_\mu \leq 100g_e$. The calculation yield the bounds represented by the black dotted curves in Figs. 2 and 3. As expected, these bounds are practically identical to those obtained for $g_\mu = g_e$ for carrier masses below 100 keV. However, they are considerably less tight for higher masses.

2.5. Bounds based on the difference $r_d^2 - r_p^2$

As observed in Section 2.1, there is excellent agreement in the value of $r_d^2 - r_p^2$ between the result derived from the measurements in μH and μD and the result derived from the isotope shift of the $1s - 2s$ interval in $e\text{H}$ and $e\text{D}$. Setting bounds on $g_e g_n$ based on these two results can be done as follows [8]. Let

$$\delta r_{\mu, \text{SM}}^2 = r_d^2 - r_p^2, \quad (8)$$

where we take r_d and r_p to be the charge radii derived from the measurements in muonic deuterium and muonic hydrogen according to standard model theory: $\delta r_{\mu, \text{SM}}^2 = 3.8200(31) \text{ fm}^2$ [15]. Similarly, let

$$\delta r_{e, \text{SM}}^2 = r_d^2 - r_p^2, \quad (9)$$

here with the difference $r_d^2 - r_p^2$ directly determined from the measurements of the isotope shift of the $1s - 2s$ interval in $e\text{D}$ and $e\text{H}$, also according to standard model theory ($\delta r_{e, \text{SM}}^2 = 3.8207(3) \text{ fm}^2$ [12]). Also, let

$$\Delta r_{2s1s}^2 = \delta r_{\mu, \text{SM}}^2 - \delta r_{e, \text{SM}}^2. \quad (10)$$

Bounds on new physics may be sought in terms of the values of $g_e g_n$ for which Δr_{2s1s}^2 differs more from zero than would be expected in view of the experimental and theoretical errors on $\delta r_{\mu, \text{SM}}^2$ and $\delta r_{e, \text{SM}}^2$.

The difference $\delta r_{e,\text{SM}}^2$ is determined by equating the experimental isotope shift of the 1s – 2s interval, $\Delta\nu_{2s1s}^{\text{exp}} = \nu_{2s1s,eD}^{\text{exp}} - \nu_{2s1s,eH}^{\text{exp}}$, to its standard model prediction, $\Delta\nu_{2s1s}^{\text{SM}} = \nu_{2s1s,eD}^{\text{SM}} - \nu_{2s1s,eH}^{\text{SM}}$. The latter can be written as

$$\Delta\nu_{2s1s}^{\text{SM}} = \Delta\nu_{2s1s}^{\text{SM0}} + \mathcal{C}_{2s1s}\delta r_{e,\text{SM}}^2, \quad (11)$$

where $\Delta\nu_{2s1s}^{\text{SM0}}$ does not depend sensitively on r_p or r_d and $\mathcal{C}_{2s1s} = -1369.5$ kHz fm⁻². Thus

$$\delta r_{e,\text{SM}}^2 = \frac{\Delta\nu_{2s1s}^{\text{exp}} - \Delta\nu_{2s1s}^{\text{SM0}}}{\mathcal{C}_{2s1s}}. \quad (12)$$

Let us suppose that the experimental isotope shift $\Delta\nu_{2s1s}^{\text{exp}}$ would differ from $\Delta\nu_{2s1s}^{\text{SM}}$ by a new physics contribution $\Delta\nu_{2s1s}^{\text{NP}}$, and let

$$\delta r_e^2 = \frac{\Delta\nu_{2s1s}^{\text{exp}} - \Delta\nu_{2s1s}^{\text{SM0}} - \Delta\nu_{2s1s}^{\text{NP}}}{\mathcal{C}_{2s1s}} = \delta r_{e,\text{SM}}^2 - \Delta\nu_{2s1s}^{\text{NP}}/\mathcal{C}_{2s1s}. \quad (13)$$

A non-zero $\Delta\nu_{2s1s}^{\text{NP}}$ would make δr_e^2 a better approximation of the true value of $r_d^2 - r_p^2$ than $\delta r_{e,\text{SM}}^2$. If we now assume that the new physics interaction does not significantly affect the measurements in the muonic species, then equating δr_e^2 to $\delta r_{\mu,\text{NP}}^2$ gives

$$\Delta r_{2s1s}^2 = \Delta\nu_{2s1s}^{\text{NP}}/\mathcal{C}_{2s1s}. \quad (14)$$

The results presented in section 2.4 indicate that this assumption is unsafe for $m_{X_0} > 100$ keV. Accordingly, we do not consider this high mass region here. Below 100 keV, however, a possible dependence of $r_d^2 - r_p^2$ on g_μ seems unlikely. Therefore, in common with [8], we take g_μ to be zero in the present approach.

Apart from negligible differences in the wave functions arising from the different reduced masses, $\Delta\nu_{2s1s}^{\text{NP}}$ is proportional to the difference $g_e g_d - g_e g_p$, which is $g_e g_n$. We write

$$\Delta\nu_{2s1s}^{\text{NP}} = (g_e g_d - g_e g_p)\Delta\tilde{\nu}_{2s1s}^{\text{NP}} = g_e g_n \Delta\tilde{\nu}_{2s1s}^{\text{NP}}, \quad (15)$$

where $\Delta\tilde{\nu}_{2s1s}^{\text{NP}}$ does not depend on g_e or g_n . We also set¶

$$\sigma_{g_e g_n} = \left| \frac{\mathcal{C}_{2s1s}\sigma_{2s1s}}{\Delta\tilde{\nu}_{2s1s}^{\text{NP}}} \right|, \quad (16)$$

where σ_{2s1s} is the combined experimental and theoretical error on $\delta r_{\mu,\text{SM}}^2 - \delta r_{e,\text{SM}}^2$. Assuming that Δr_{2s1s}^2 is not affected by systematic or random errors not taken into account through σ , Eq. (14) then implies that

$$\frac{\mathcal{C}_{2s1s}\Delta r_{2s1s}^2}{\Delta\tilde{\nu}_{2s1s}^{\text{NP}}} - 1.96\sigma_{g_e g_n} \leq g_e g_n \leq \frac{\mathcal{C}_{2s1s}\Delta r_{2s1s}^2}{\Delta\tilde{\nu}_{2s1s}^{\text{NP}}} + 1.96\sigma_{g_e g_n} \quad (17)$$

¶ Apart from insignificant numerical differences beyond an overall factor of 1.96, the quantity $\sigma_{g_e g_n}$ defined by this equation is equivalent to the sensitivity parameter $\sigma(|g_e g_p|)$ defined by Eq. (30) of [10] if g_d is taken to be $2g_p$ when calculating the latter.

at the 95% confidence level. The precision on the value of $g_e g_n$ obtained in this way is thus determined by $\sigma_{g_e g_n}$. This quantity can also be understood as quantifying the sensitivity of the method to a non-zero value of $g_e g_n$.

The bounds given by Eq. (17) are also plotted in Fig. 3, where they are represented by the solid orange curves. Up to masses of about 100 keV, these results are practically identical to the bounds represented by the long-dashed curves, which are based on the same experimental data but are obtained differently. The significant differences noticeable for higher masses illustrate the importance of allowing for a possible new physics contribution to the Lamb shift of the muonic species in that region.

3. Extension to ${}^3\text{He}$ and ${}^4\text{He}$

As discussed in [8], setting bounds based on individual helium transition frequencies is hampered by relatively large experimental or theoretical uncertainties for most of these transitions. However, the approach to bounding $g_e g_n$ outlined in Section 2.5 can be immediately extended to helium, now working with the difference of the squares of the rms charge radii of ${}^3\text{He}$ and ${}^4\text{He}$, $r_h^2 - r_\alpha^2$, rather than with $r_d^2 - r_p^2$ [8]. The necessary experimental isotope shifts are available for three different intervals, i.e., the $2{}^3\text{S} - 2{}^1\text{S}$ and $2{}^3\text{S} - 2{}^3\text{P}$ intervals, and, with a much lower precision, the $2{}^1\text{S} - 3{}^1\text{D}$ interval. This approach also avoids the need of taking into account a possible new physics interaction between the two electrons (see, e.g., Appendix A).

Measurements in muonic ${}^3\text{He}$ and muonic ${}^4\text{He}$ have resulted in a value of $1.0636(31) \text{ fm}^2$ for $r_h^2 - r_\alpha^2$ [13, 15, 18], or $1.0626(29) \text{ fm}^2$ as redetermined in [19]. The most precise determination of $r_h^2 - r_\alpha^2$ in the electronic species to date, $1.0678(7) \text{ fm}^2$, is based on recent measurements of the $2{}^3\text{S} - 2{}^1\text{S}$ interval in helium-3 [17] and helium-4 [39], combined with theory [16, 20, 40]; this value differs by 1.3σ and 1.7σ from those deduced from the muonic species in, respectively, [18] and [19] — Fig. 1(c). The result derived from a previous measurement of that interval in helium-3 [41] also agrees with these two values but has a much larger uncertainty [17]. Three experimental values of the $2{}^3\text{S} - 2{}^3\text{P}$ isotope shift are currently available [40, 42, 43, 44, 45]. Two give values of $r_h^2 - r_\alpha^2$ in excellent agreement with the value of $1.0636(31) \text{ fm}^2$ derived from the measurements on the muonic species but are in 2σ tension with each other. The third one gives a considerably different result, $1.028(2) \text{ fm}^2$ [45]. The value derived from the $2{}^1\text{S} - 3{}^1\text{D}$ interval, $1.059(25) \text{ fm}^2$ [46], is also in agreement with the muonic value but has a considerably larger uncertainty.

We focus on the difference $r_h^2 - r_\alpha^2$ between the squared nucleus rms charge radii of ${}^3\text{He}$ and that of ${}^4\text{He}$, rather than on the difference $r_d^2 - r_p^2$. Proceeding as in Section 2.5 yields the 95%-percent confidence bound

$$\frac{C_{ba}\Delta r_{ba}^2}{-\Delta\tilde{\nu}_{ba}^{\text{NP}}} - 1.96\sigma_{g_e g_n} \leq g_e g_n \leq \frac{C_{ba}\Delta r_{ba}^2}{-\Delta\tilde{\nu}_{ba}^{\text{NP}}} + 1.96\sigma_{g_e g_n}. \quad (18)$$

Here Δr_{ba}^2 is the difference between the value of $r_h^2 - r_\alpha^2$ derived from measurements in muonic helium ($\delta r_{\mu,\text{SM}}^2$) and the value of this quantity derived from measurements of

Table 1. Data used in the present work. We assume that $\delta r_{\mu, \text{SM}}^2 = 3.8200(31) \text{ fm}^2$ for muonic hydrogen [15] and $1.0626(29) \text{ fm}^2$ for muonic helium [19]. For $\delta r_{e, \text{SM}}^2$, we use the results of [12] for the $1s - 2s$ interval, the results of van der Werf *et al* [16, 17] for the $2^3\text{S} - 2^1\text{S}$ interval, and the results of Shiner *et al* [40, 42] and Cancio Pastor *et al* [40, 43, 44] for the $2^3\text{S} - 2^3\text{P}$ interval. The values of \mathcal{C}_{ba} for helium are taken from [40].

Interval	$\delta r_{e, \text{SM}}^2 \text{ (fm}^2\text{)}$	$\Delta r_{ba}^2 \text{ (fm}^2\text{)}$	$\sigma_{ba} \text{ (fm}^2\text{)}$	$\mathcal{C}_{ba} \text{ (kHz fm}^{-2}\text{)}$
$1s - 2s$	3.8207(3)	-0.0007	0.0031	-1369.5
$2^3\text{S} - 2^1\text{S}$	1.0678(7)	-0.0052	0.0030	-214.66
$2^3\text{S} - 2^3\text{P (S)}$	1.061(3)	0.002	0.004	-1212.2
$2^3\text{S} - 2^3\text{P (CP)}$	1.069(3)	-0.006	0.004	-1212.2

the isotope shift of the $a - b$ interval in electronic ^3He and ^4He according to standard model theory ($\delta r_{e, \text{SM}}^2$). Moreover,

$$\sigma_{g_e g_n} = \left| \frac{\mathcal{C}_{ba} \sigma_{ba}}{\Delta \tilde{\nu}_{ba}^{\text{NP}}} \right|, \quad (19)$$

where σ_{ba} is the combined experimental and theoretical error on Δr_{ba}^2 . The minus signs in the denominators arise from the definition of the new physics contribution to the isotope shift, $\Delta \nu_{ba}^{\text{NP}}$, which we take to be $\nu_{ba, ^3\text{He}}^{\text{NP}} - \nu_{ba, ^4\text{He}}^{\text{NP}}$ for consistency with the usual definition of the isotope shift for these intervals and the sign of \mathcal{C}_{ba} : here

$$\Delta \nu_{ba}^{\text{NP}} = (g_e g_h - g_e g_\alpha) \Delta \tilde{\nu}_{ba}^{\text{NP}} = -g_e g_n \Delta \tilde{\nu}_{ba}^{\text{NP}}. \quad (20)$$

We use the values of \mathcal{C}_{ba} , Δr_{ba}^2 and σ_{ba} listed in Table 3 (we do not consider the $2^1\text{S} - 3^1\text{D}$ interval in view of the large uncertainty on its isotope shift). The calculation of $\Delta \tilde{\nu}_{ba}^{\text{NP}}$ is outlined in Appendix A.

The resulting values of $\sigma_{g_e g_n}$ are plotted in Fig. 4, both for helium and for the $1s - 2s$ interval of hydrogen. The form of $V_{\text{NP}}(r)$ implies that in the $m_{X_0} \rightarrow 0$ limit

$$\sigma_{g_e g_n} \propto \left| \frac{\mathcal{C}_{ba} \sigma_{ba}}{n \langle b | 1/r | b \rangle - n \langle a | 1/r | a \rangle} \right|, \quad (21)$$

where n is the number of electrons. \mathcal{C}_{ba} is larger for the $1s - 2s$ interval of hydrogen than for the two intervals of helium considered here. However, the denominator of Eq. (21) is considerably smaller for the latter [47], with the consequence that a greater sensitivity is obtained in the low mass region by using the $1s - 2s$ interval. As can be seen from the figure, this is also the case beyond that region. Bounds based on the isotope shift of these two helium intervals can therefore be expected to be less tight than the bounds based on the $1s - 2s$ interval.

The sensitivity to a non-zero value of $g_e g_n$ of the King plots analysis of [2] and of the of World data results of Section 2.3 is also indicated in Fig. 4. For these two approaches, we take $\sigma_{g_e g_n}$ to be half the width of the respective 95% confidence interval on the value

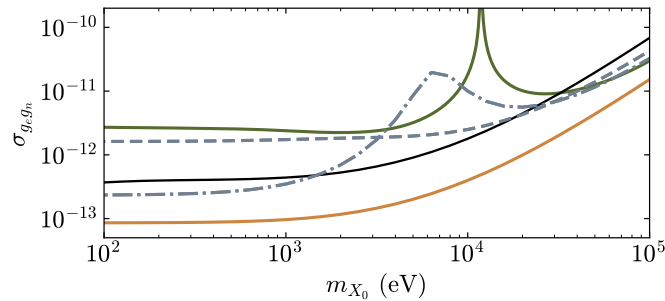


Figure 4. The sensitivity parameter $\sigma_{g_e g_n}$ of Eqs. (16) and (19) as derived from the isotope shift of the $1s - 2s$ interval in hydrogen (solid orange curve), from the isotope shift of the $2^3S - 2^1S$ interval of He (dash-dotted curve) or from the isotope shift of the $2^3S - 2^3P$ interval of He (short-dashed curve). The solid green curve and solid black curve indicate the corresponding values of $\sigma_{g_e g_n}$ for, respectively, the King plots analysis of [2] and the World data results of Section 2.3, as explained in the text.

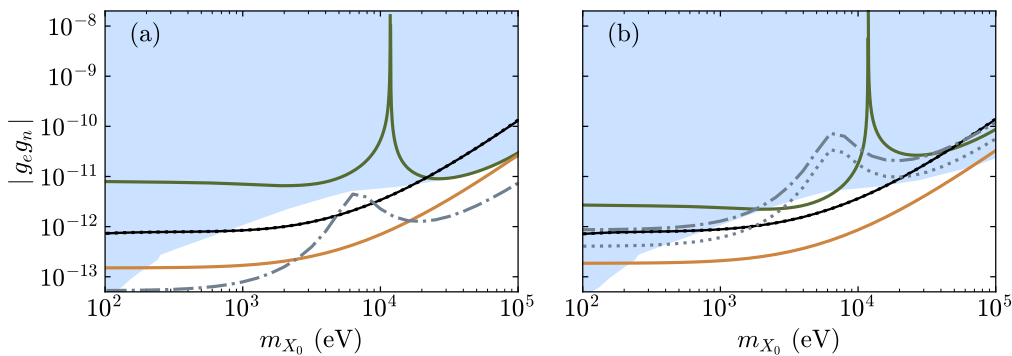


Figure 5. As in Fig. 3, here with dash-dotted curves indicating the bounds on $g_e g_n$ based on the isotope shift of the $2^3S - 2^1S$ interval of He. The dotted curve in (b) is the value of $g_e g_n$ for which the new physics shift would entirely explain the difference between $\delta r_{\mu, \text{SM}}^2$ and $\delta r_{e, \text{SM}}^2$.

of $g_e g_n$, divided by 1.96 for consistency with Eqs. (16) and (19). The comparison points to a greater sensitivity of the spectroscopy of hydrogen and, to a lesser extent, of helium.

The bounds on the value of $g_e g_n$ predicted by Eq. (18) for the $2^3S - 2^1S$ interval are shown in Fig. 5, where they are represented by dash-dotted curves (the corresponding results for the $2^3S - 2^3P$ interval are presented in the Supplementary Material, for completeness). These bounds are not symmetrical around $g_e g_n = 0$ because of the significant difference between $\delta r_{\mu, \text{SM}}^2$ and $\delta r_{e, \text{SM}}^2$ for this interval, with the result that the $2^3S - 2^1S$ bound tends to be particularly tight in Fig. 5(a). However, this difference seems too large to be primarily due to a new physics shift, if there would be any suspicion that a fifth force might be at play here, as can be surmised from the dotted curve indicating the centre of the confidence interval defined by Eq. (21). The values of $g_e g_n$ represented

by this curve are larger than the corresponding $1s - 2s$ bound (the solid orange curve), and are therefore excluded by it. Taking the $2^3S - 2^1S$ bound of Fig. 5(a) at face value would therefore be imprudent. Nonetheless, it is worth noting that these helium results are broadly consistent with the bounds derived from hydrogen and deuterium spectroscopy.

4. Conclusions

In summary, we have presented newly calculated bounds on the products $g_e g_p$ and $g_e g_n$ derived from the high precision spectroscopic data currently available for hydrogen, deuterium, helium-3 and helium-4. These results update those of [8] and build up on our previous work on the topic [9, 10]. They do not depend on a specific assumption on the ratio g_d/g_p (or on the ratio g_α/g_h in helium), contrary to the confidence intervals on $g_e g_p$ presented in [10]. They do depend on the ratio g_μ/g_e , but in a minor if not completely negligible way for carrier masses below 100 keV if $|g_\mu|$ is assumed not to be several order of magnitude larger than $|g_e|$.

In this mass region, the bounds on $g_e g_n$ based on the World spectroscopic data for hydrogen and deuterium tend to be more stringent than the bounds arising from the analysis of King plots nonlinearities, in the current state of development of that approach [2, 3, 4]. However, they are impacted by the well known inconsistencies between the available data. As was already pointed out in [8], particularly stringent bounds can be set by combining the isotope shift of the $1s - 2s$ interval in eH and eD with the rms charge radii of the proton and the deuteron derived from the measurements of the Lamb shift in μH and μD . However, being based on a relatively small number of experiments, these results might conceivably be affected by unknown systematic errors.

Setting bounds based on the isotope shift of particular intervals in helium is also possible, and results in bounds broadly consistent with those obtained for hydrogen and deuterium. The approach is less powerful for helium, though, because of the smaller new physics shift of the intervals for which sufficiently precise isotope shifts are available.

The theoretical error on the value of $r_d^2 - r_p^2$ derived from muonic hydrogen and muonic deuterium is the main limitation on the sensitivity of the bounds based on the isotope shift of the $1s - 2s$ interval in hydrogen and deuterium. Lowering this theoretical error would thus make it possible to strengthen these bounds further. Alternatively, the same could also be achieved by combining the isotope shift of this interval with that of another interval, which would also bypass the need of using the muonic species data and therefore eliminate the dependence of these bounds on the value of g_μ [8, 10].

Acknowledgements

This work much benefitted from conversations with M P A Jones and M Spannowsky and communications from K Pachucki. The programs used in the helium calculations are based on codes written by B Yang, M Pont, T Li and R Shakeshaft and kindly

provided to the author by R Shakeshaft a number of years ago.

Appendix A. Calculation of the new physics frequency shifts

A new physics interaction of the type considered in this work would potentially affect the experimental transition frequencies by shifting the energies of the respective states from their standard model values. The contribution ν_{ba}^{NP} this interaction would make to the transition frequency of a transition between a state a and a state b would be

$$\nu_{ba}^{\text{NP}} = (\delta E_b^{\text{NP}} - \delta E_a^{\text{NP}})/h, \quad (\text{A.1})$$

in terms of the new physics shifts δE_a^{NP} and δE_b^{NP} of the energies of the respective states and of the Planck's constant h . Since the potential $V_{\text{NP}}(r)$ is certainly very weak compared to the Coulomb potential, if non-zero, the energy shifts δE_a^{NP} , δE_b^{NP} , \dots , do not need to be calculated beyond first order perturbation theory [5, 6, 7].

Accordingly, we simply set, for electronic hydrogen and deuterium,

$$\delta E_a^{\text{NP}} = \int \psi_a^*(\mathbf{r}) V_{\text{NP}}(r) \psi_a(\mathbf{r}) \, \text{d}\mathbf{r}, \quad \delta E_b^{\text{NP}} = \int \psi_b^*(\mathbf{r}) V_{\text{NP}}(r) \psi_b(\mathbf{r}) \, \text{d}\mathbf{r}, \quad (\text{A.2})$$

where $\psi_a(\mathbf{r})$ and $\psi_b(\mathbf{r})$ are the unperturbed non-relativistic wave functions of the corresponding bound states. As in [9, 10], we calculate these energy shifts either analytically or numerically, in the latter case by obtaining the wave functions by diagonalising the matrix representing the unperturbed Hamiltonian in a Sturmian basis. For muonic hydrogen and muonic deuterium, we use relativistic wave function obtained by solving the Dirac equation for a muon in the Coulomb and Uehling potentials of an extended nuclear charge distribution, as in [10].

A similar calculation for helium would normally involve computing matrix elements of the new physics electron-electron interaction, besides computing the matrix elements of $V_{\text{NP}}(r)$ for each of the electrons. A method for doing this is described in [8]. In the present work, however, we only consider the effect of the new physics interaction on the isotope shift of transitions in electronic ^3He and ^4He . We only need to calculate $\Delta\nu_{ba}^{\text{NP}}$ for the relevant transitions, thus, rather than individual new physics energy shifts. In terms of the latter,

$$\Delta\nu_{ba}^{\text{NP}} = [(\delta E_{b,^3\text{He}} - \delta E_{a,^3\text{He}}) - (\delta E_{b,^4\text{He}} - \delta E_{a,^4\text{He}})]/h. \quad (\text{A.3})$$

At the level of the Schrödinger equation, the contribution of the new physics electron-electron interaction to the energy shift of a same state differs between ^3He and ^4He only because of the different nuclear masses of these two isotopes, which impact on the wave functions through reduced mass and mass polarisation corrections. These differences are negligible for our purpose. Hence, only the electron-nucleus new physics interaction needs to be taken into account in the isotope shifts. In this approximation, and assuming

that $g_\alpha - g_h = g_n$ as noted above,

$$\delta E_{a,4\text{He}} - \delta E_{a,3\text{He}} = (-1)^{s+1} g_e g_n \int \psi_a^*(\mathbf{r}_1, \mathbf{r}_2) \left[\tilde{V}_{\text{NP}}(r_1) + \tilde{V}_{\text{NP}}(r_2) \right] \psi_a(\mathbf{r}_1, \mathbf{r}_2) d\mathbf{r}_1 d\mathbf{r}_2, \quad (\text{A.4})$$

and similarly for the difference $\delta E_{b,4\text{He}} - \delta E_{b,3\text{He}}$. In this equation, \mathbf{r}_1 and \mathbf{r}_2 are the position vectors of the two electrons, $\psi_a(\mathbf{r}_1, \mathbf{r}_2)$ is the unperturbed non-relativistic wave function of state a for an infinite nuclear mass, and

$$\tilde{V}_{\text{NP}}(r) = \frac{1}{4\pi} \frac{1}{r} \exp(-m_{X_0} r). \quad (\text{A.5})$$

An accurate calculation requires correlated two-electron wave functions [8]. We use wave functions obtained by diagonalising the unperturbed Hamiltonian in a Laguerre basis expressed in perimetric coordinates, following [48] and more recently [49, 50]. Specifically, we use a basis of antisymmetrized products of an angular factor and radial functions of the following form [49, 50],

$$\phi_{lmn}(u, v, w) = \exp[-(k_1 u + k_2 v + k_3 w)/2] L_l(k_1 u) L_m(k_2 v) L_n(k_3 w), \quad (\text{A.6})$$

where $L_p(\cdot)$ denotes the Laguerre polynomial of order p , k_1 and k_2 are two scaling constants, $k_3 = (k_1 + k_2)/2$, and

$$u = r_2 + r_3 - r_1, \quad v = r_1 + r_3 - r_2, \quad w = 2(r_1 + r_2 - r_3) \quad (\text{A.7})$$

with $r_3 = |\mathbf{r}_1 - \mathbf{r}_2|$. We set $k_1 = 2.01 a_0^{-1}$ and $k_2 = 0.765 a_0^{-1}$, where a_0 is the Bohr radius. This choice, while presumably not optimal, ensured that the expectation value of the new physics potential converged to between four and seven significant figures, depending on the state and on m_{X_0} , when the basis was increased to the maximum size used in the computation ($l + m + n \leq 10$ for the 2^1S state, ≤ 8 for the 2^3S state and ≤ 15 for the 2^3P state). These parameters also ensured that the corresponding values of $\langle 1/r \rangle$ matched the benchmark results of [47] to five significant figures.

References

- [1] Berengut J C, Budker D, Delaunay C, Flambaum V V, Frugiuele C, Fuchs E, Grojean C, Harnik R, Ozeri R, Perez G and Soreq Y 2018 Probing new long-range interactions by isotope shift spectroscopy *Phys. Rev. Lett.* **120** 091801
- [2] Hur J *et al* 2022 Evidence of two-source King plot nonlinearity in spectroscopic search for new boson *Phys. Rev. Lett.* **128** 163201
- [3] Door M *et al* 2024 Search for new bosons with ytterbium isotope shifts. <https://doi.org/10.48550/arXiv.2403.07792>
- [4] Wilzewski A *et al* 2024 Nonlinear calcium King plot constrains new bosons and nuclear properties. <https://doi.org/10.48550/arXiv.2412.10277>
- [5] Jaeckel J and Roy S 2010 Spectroscopy as a test of Coulomb's law: A probe of the hidden sector *Phys. Rev. D* **82** 125020
- [6] Karshenboim S G 2010 Constraints on a long-range spin- independent interaction from precision atomic physics *Phys. Rev. D* **82** 073003.

- [7] Brax P and Burrage C 2011 Atomic precision tests and light scalar couplings *Phys. Rev. D* **83** 035020
- [8] Delaunay C, Frugiuele C, Fuchs E and Soreq Y 2017 Probing new spin-independent interactions through precision spectroscopy in atoms with few electrons *Phys. Rev. D* **96** 115002
- [9] Jones M P A, Potvliege R M and Spannowsky M 2020 Probing new physics using Rydberg states of atomic hydrogen *Phys. Rev. Res.* **2** 013244
- [10] Potvliege R M, Nicolson A, Jones M P A and Spannowsky M 2023 Deuterium spectroscopy for enhanced bounds on physics beyond the standard model *Phys. Rev. A* **108** 052825
- [11] Delaunay C, Karr J-P, Kitahara T, Koelemeij J C J, Soreq Y and Zupan J 2023 Self-consistent extraction of spectroscopic bounds on light new physics *Phys. Rev. Lett.* **130** 121801
- [12] Pachucki K, Partkóš V and Yerokhin V A 2018 Three-photon-exchange nuclear structure correction in hydrogenic systems *Phys. Rev. A* **97** 062511
- [13] Krauth J J *et al* 2021 Measuring the α -particle charge radius with muonic helium-4 ions *Nature* **589** 527
- [14] Lensky V, Hagelstein F and Pascalutsa V 2022 A reassessment of nuclear effects in muonic deuterium using pionless effective field theory at N³LO *Phys. Lett. B* **835** 137500
- [15] Pachucki K, Lensky V, Hagelstein F, Li Muli S S, Bacca S and Pohl R 2024 Comprehensive theory of the Lamb shift in light muonic atoms *Rev. Mod. Phys.* **96** 015001
- [16] Pachucki, K, Partkóš V and Yerokhin V A 2024 Second-order hyperfine correction to H, D and ³He energy levels *Phys. Rev. A* **110** 062806
- [17] van der Werf Y, Steinebach K, Jannin R, Bethlem H L and Eikema K S E 2023 The alpha and helion particle charge radius difference from spectroscopy of quantum-degenerate helium. <https://doi.org/10.48550/arXiv.2306.02333>
- [18] Schuhmann K *et al* (the CREMA Collaboration) 2023 The helion charge radius from laser spectroscopy of muonic helium-3 ions. <https://doi.org/10.48550/arXiv.2305.11679>
- [19] Li Muli C C, Richardson T R and Bacca S 2024 Revisiting the helium isotope-shift puzzle with improved uncertainties from nuclear structure corrections. <https://doi.org/10.48550/arXiv.2401.13424>
- [20] Qi X-Q, Zhang P-P, Yan Z-C, Tang L-Y, Chen A-X, Shi T-Y and Zhong Z-X 2024 Revised ³He nuclear charge radius due to electronic hyperfine mixing. <https://doi.org/10.48550/arXiv.2409.09279>
- [21] Khabarova K Y and Kolachevsky N N 2021 Proton charge radius *Usp. Fiz. Nauk* **191** 1095 [*Phys. Usp.* **64** 1038]
- [22] Hiyama E and Suzuki T 2024 Moments of the charge distribution observed through electron scattering in ³H and ³He *Prog. Theor. Exp. Phys.* **2024** 083D02
- [23] Tiesinga E, Mohr P J, Newell D B and Taylor B N 2021 CODATA recommended values of the fundamental physical constants: 2018 *Rev. Mod. Phys.* **93** 025010
- [24] Brandt A D, Cooper S F, Rasor C, Burkley Z, Matveev A and Yost D C 2022 Measurement of the 2S_{1/2}–8D_{5/2} transition in hydrogen 2022 *Phys. Rev. Lett.* **128** 023001.
- [25] Scheidegger S and Merkt F 2024 Precision-spectroscopic determination of the binding energy of a two-body quantum system: The hydrogen atom and the proton-size puzzle *Phys. Rev. Lett.* **132** 113001
- [26] Antognini A *et al* 2013 Proton structure from the measurement of 2S – 2P transition frequencies of muonic hydrogen *Science* **339** 417
- [27] Parthey C G *et al* 2011 Improved measurement of the hydrogen 1S – 2S transition frequency *Phys. Rev. Lett.* **107** 203001
- [28] Matveev A *et al* 2013 Precision measurement of the hydrogen 1S – 2S frequency via a 920-km fiber link *Phys. Rev. Lett.* **110** 230801
- [29] Grinin A, Matveev A, Yost D C, Maisenbacher L, Wirthl V, Pohl R, Hänsch T W, Udem T 2020 Two-photon frequency comb spectroscopy of atomic hydrogen *Science* **370** 1061
- [30] Fleurbaey H, Galtier S, Thomas S, Bonnaud M, Julien L, Biraben F and Nez F 2018 New

- measurement of the $1S - 3S$ transition frequency of hydrogen: Contribution to the proton charge radius puzzle *Phys. Rev. Lett.* **120** 183001
- [31] de Beauvoir B, Nez F, Julien L, Cagnac B, Biraben F, Touahri D, Hilico L, Acef O, Clairon A and Zondy J J 1997 Absolute frequency measurement of the $2S - 8S/D$ transitions in hydrogen and deuterium: New determination of the Rydberg constant *Phys. Rev. Lett.* **78** 440
- [32] Bezginov N, Valdez T, Horbatsch M, Marsman A, Vutha A C and Hessels E A 2019 A measurement of the atomic hydrogen Lamb shift and the proton charge radius *Science* **365** 1007
- [33] Beyer A *et al* 2017 The Rydberg constant and proton size from atomic hydrogen *Science* **358** 79
- [34] Pohl R *et al* 2016 Laser spectroscopy of muonic deuterium *Science* **353** 669
- [35] Parthey C G, Matveev A, Alnis J, Pohl R, Udem T, Jentschura U D, Kolachevsky N and Hänsch T W 2010 Precision measurement of the hydrogen-deuterium $1S - 2S$ isotope shift *Phys. Rev. Lett.* **104** 233001
- [36] Jentschura U D, Matveev A, Parthey C G, Alnis J, Pohl R, Udem T, Kolachevsky N and Hänsch T W 2011 Hydrogen-deuterium isotope shift: From the $1S - 2S$ -transition frequency to the proton-deuteron charge-radius difference *Phys. Rev. A* **83** 042505
- [37] Mohr P J and Taylor B N 2000 CODATA recommended values of the fundamental physical constants: 1998 *Rev. Mod. Phys.* **72** 351
- [38] Mohr P J, Newell D B and Taylor B N 2016 CODATA recommended values of the fundamental physical constants: 2014 *Rev. Mod. Phys.* **88** 035009
- [39] Rengelink R J, van der Werf Y, Notermans R P M J W, Jannin R, Eikema K S E, Hoogerland M D and Vassen W 2018 Precision spectroscopy of helium in a magic wavelength optical dipole trap *Nature Phys.* **14** 1132
- [40] Pachucki K, Partkoš V and Yerokhin V A 2017 Testing fundamental interactions on the helium atom *Phys. Rev. A* **95** 062510
- [41] van Rooij R, Borbely J S, Simonet J, Hoogerland M D, Eikema K S E, Rozendaal R A and Vassen W 2011 Frequency metrology in quantum degenerate helium: Direct measurement of the $2^3S_1 \rightarrow 2^1S_0$ transition *Science* **333** 196
- [42] Shiner D, Dixon R and Vedantham V 1995 Three-nucleon charge radius: A precise laser determination using ^3He *Phys. Rev. Lett.* **74** 3553
- [43] Cancio Pastor P, Giusfredi G, De Natale P, Hagel G, de Mauro C and Inguscio M 2012 Absolute frequency measurements of the $2^3S_1 \rightarrow 2^3P_{0,1,2}$ atomic helium transitions around 1083 nm *Phys. Rev. Lett.* **92** 023001; *ibid.* **97** 139903(E)
- [44] Cancio Pastor P, Consolino L, Giusfredi G, De Natale P, Inguscio M, Yerokhin V A and Pachucki K 2012 Frequency metrology of helium around 1083 nm and determination of the nuclear charge radius *Phys. Rev. Lett.* **108** 143001
- [45] Zheng X, Sun Y R, Chen J-J, Jiang W, Pachucki K and Hu S-M 2017 Measurement of the frequency of the $2^3S - 2^3P$ transition of ^4He *Phys. Rev. Lett.* **119** 263002
- [46] Huang Y-J, Guan Y-C, Peng J-L, Shy J-T and Wang L-B 2020 Precision laser spectroscopy of the $2^1S_0 - 3^1D_2$ two-photon transition in ^3He *Phys. Rev. A* **101** 062507
- [47] Davis B F and Chung K T 1982 Mass-polarization effect and oscillator strengths for S, P, D states of helium *Phys. Rev. A* **25** 1328
- [48] Pekeris C L 1958 Ground state of two-electron atoms *Phys. Rev.* **112** 1649
- [49] Yang B, Pont M, Shakeshaft R, van Duijn E and Piraux, B 1997 Description of a two-electron atom or ion in an ac field using interparticle coordinates, with an application to H^- *Phys. Rev. A* **56** 4946
- [50] Li T and Shakeshaft R 2005 S-wave resonances of the negative positronium ion and stability of a system of two electrons and an arbitrary positive charge *Phys. Rev. A* **71** 052505

Spectroscopy of light atoms and bounds on physics beyond the standard model

Supplementary material

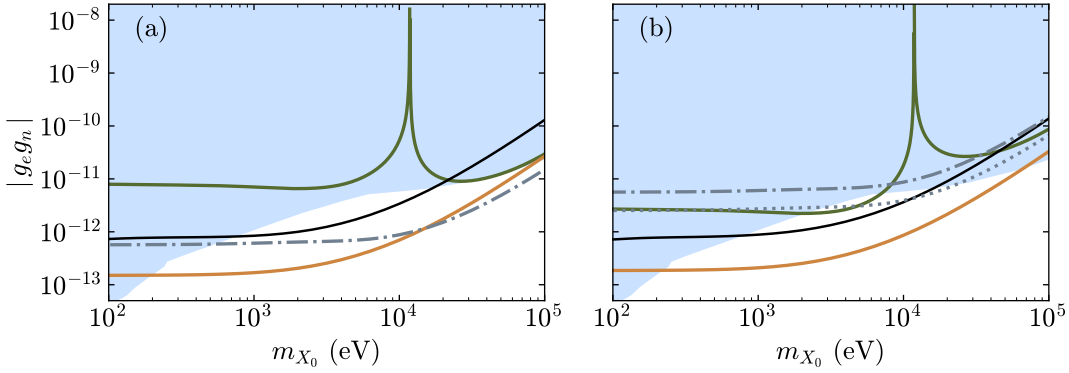


Figure A1. The same as Fig. 5 of the main text, but here with the dash-dotted and dotted curves referring to the bounds on $g_e g_n$ calculated from the isotope shift of the $2^3\text{S} - 2^3\text{P}$ interval based on the results of Cancio Pastor *et al.*

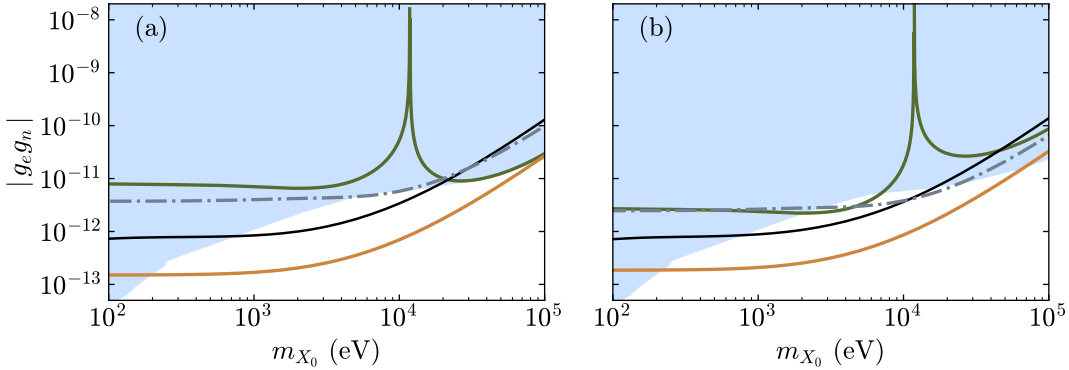


Figure A2. The same as Fig. 5 of the main text, but here with the dash-dotted curves referring to the bounds on $g_e g_n$ calculated from the isotope shift of the $2^3\text{S} - 2^3\text{P}$ interval based on the results of Shiner *et al.* There is no dotted curve representing the centre of the confidence interval here, as these values of $g_e g_n$ fall below the bottom of the graphs.